Optimization-Based Design Model for Electric Traction Motors Considering the Supply Risk of Critical Materials

JESÚS R. PÉREZ-CARDONA [1,2], **JOHN W. SUTHERLAND** [1,2],
AND SCOTT D. SUDHOFF [3] **(Fellow, IEEE)**

[1]School of Environmental and Ecological Engineering, Purdue University, West Lafayette, IN 47907 USA
[2]Critical Materials Institute (CMI), USA
[3]Department of Electrical and Computer Engineering, Purdue University, West Lafayette, IN 47907 USA
CORRESPONDING AUTHOR: J. R. PÉREZ-CARDONA (jperezc@purdue.edu)

ABSTRACT Electric Vehicles (EVs) are considered among one of the 'clean' energy technologies in the transportation sector because the vehicles themselves do not generate combustion emissions. However, the substantial environmental footprint associated with the materials needed to create these technologies (extraction, manufacturing, and solid waste at end of life) calls into question their 'clean' label. In addition, their increasing demand adds to the existing supply risk (SR) through the requirement of critical materials. To address this, the purpose of this study is to establish a design model for electric traction motors, which are used in EVs, that will address the SR issues early in the design stage. The design model incorporates a genetic algorithm with the following objectives: minimum motor mass, minimum energy consumption, and minimum SR-equivalent. The SR-equivalent objective prioritizes the minimization of materials with high SR. Using the case study of a surface-mounted permanent magnet synchronous motor, results show how each objective is related to each other and to the parameters chosen as variables. Further analysis shows the benefits of minimizing for SR-equivalent of required materials. Future work is needed to improve the design model in terms of other important metrics such as minimizing environmental impact and cost.

INDEX TERMS Machine design, multi-objective optimization, surface-mounted permanent-magnet machine, supply risk, sustainable design.

I. INTRODUCTION

DEVELOPING clean energy technologies is one approach for moving towards sustainability [1]. The primary benefit of such technologies is that they reduce the lifecycle environmental footprint of a product, process, or service by improving energy efficiency, avoiding non-renewable resources, reducing waste, reusing materials, etc. These technologies may also help contribute to other economic and social needs. In the transportation sector, electric vehicles (EVs) represent a promising alternative to reduce greenhouse gas (GHG) emissions from internal combustion engine vehicles powered by fossil fuels. EVs are known as 'clean' energy technologies because they emit zero GHGs at point of use (of course, the production of electricity that powers an EV may have a substantial GHG footprint). Other clean energy technologies include wind turbines and photovoltaic solar panels.

While clean energy technologies hold the promise of benefits in terms of GHG reduction, they are not without challenges. For example, they may incur increased environmental burdens in other stages of their life cycles; thus, research is needed to reduce these environmental impacts. In the case of EVs, the powertrain system requires a powerful electric traction motor(s) and a high-capacity energy storage system (e.g., lithium-ion battery pack) for satisfying design specifications (e.g., lower energy consumption and higher driving range, respectively). The production of these major components and their associated need for critical materials incur new environmental burdens that did not exist with conventional vehicles powered by fossil fuels.

Another consequence of clean energy technologies is the supply risk (SR) associated with nonfuel mineral commodities that are needed for their production [2], [3]. According to a recent publication, the 2022 list of mineral commodities considered critical to the United States economy and national security has increased to fifty materials [4]. Not all of these critical materials are subject to a similar SR level, but have some level of potential disruption, economic vulnerability, or trade exposure across the supply chain. It should also be noted that materials SR, as one of the three dimensions of materials criticality, is a dynamic characteristic [5].

Among the materials used in EVs, most of the critical materials subject to high SRs are in the batteries and motors when permanent magnets (PMs) are used in the vehicles. Lithium-ion batteries use lithium, cobalt, graphite, and manganese [6]. Depending on the PMs employed in the motor, varying rare earth elements (REE) and other critical materials are used. For example, Nd-Fe-B magnets may use neodymium, dysprosium, and praseodymium; Sm-Co magnets use samarium and cobalt; and Al-Ni-Co magnets use aluminum, nickel, and cobalt [7], [8]. However, batteries and motors should not be the only components considered when talking about SR. Other components such as the EV body is commonly made of aluminum and frame of the motor can be made of aluminum, cast iron, or steel [9]. Even though the United States does not suffer a high disruption potential for aluminum, it experiences high economic vulnerability and trade exposure, and aluminum is the 8th (out of 50) most critical material [3], [10].

The challenges encountered in clean energy technologies (new environmental burden and supply risk) when compared against competitive products found in the market suggests that there is a need for engineers to address these issues early at the design stage of a product.

To explore this issue, this research paper studies the design of electric traction motors applied such as would be used for an EV. The paper has two main goals. The first goal is to present a design methodology for optimizing electric traction motors. The second goal is to define a quantitative method for calculating an SR-equivalent score of materials and components for any target product. To our knowledge, this is the first paper that proposes a general function for minimizing the SR for all critical materials and a method for addressing this issue at the engineering design stage. Minimizing this function proved to be useful, because it was seen that minimizing the mass of the motor is not the same as minimizing the SR. This paper is organized as follows. First, a brief literature review describes various strategies for reducing reliance on high SR materials. Following this brief review, the design framework, model, and calculations are described. Then the results from applying the design framework to a case study are discussed. This section will illustrate the importance of choosing the proper objective functions. Finally, the paper will summarize, and conclusions will be offered.

II. DESIGN STRATEGIES FOR ELECTRIC TRACTION MOTORS

For many applications and over the course of many years, new technologies have been proposed for products that call for innovations, e.g., new materials, new processes, and new methods. When new materials / elements are called for, this often has an associated increased materials SR. However, efforts by the research community have proposed design feedbacks to reduce the demand for these critical materials. Different strategies to decrease the SR of critical materials have been delineated by the Critical Materials Institute (CMI), one of the U.S. Department of Energy's innovation hubs [2]. In summary, these strategies are 1) diversify the supply, 2) discover new materials that may substitute completely or partially, and 3) apply circular economy (reusing, recycling, etc.) principles to close material loops. Specifically, strategies 2 and 3 seek to reduce the demand for virgin critical materials. Any technology developed in response to one of these strategies must be demonstrated to be economically and environmentally competitive when compared to existing competitive technologies.

Researchers have proposed either non-rare earth permanent magnets (REPMs) or magnet-free motor topologies in an effort to improve performance and mitigate SR [9], [11]. Motors that utilize PMs (with REPMs or non-REPMs) may be configured for use in dc machines, permanent magnet synchronous motors (PMSMs), or PM-assisted synchronous reluctance machines (PMa-SynRMs) [9]. Examples of non-REPMs in development that may be used in these motors include MnAl, MnBi, Al-Ni-Co with higher energy and operating temperature, tetrataenite L10-FeNi, L10-FeCo, HfCo, ZrCo, carbides, and iron nitride. At this phase of development, the main challenge for most of these PMs, unlike REPMs, is that they cannot achieve both high remanent magnetization and high coercivity simultaneously (such properties are desirable for PM motors). The most developed non-REPMs are MnAl, MnBi, and a''-Fe16N2 [11].

The two most explored magnet-free traction motors in industry are the induction motor (IM), and the reluctance motor (RM). A main reason for EV companies using IMs is to avoid the PMs due to their high SR and cost. The main disadvantage of IMs is that they are less efficient than PMSMs due to power losses in rotor short-circuited windings. There are two types of RMs: switched and synchronous. Switched reluctance motors (SRMs) and synchronous reluctance motors (SynRMs) are magnet-free alternatives to IMs for those looking for manufacturing simplicity, and materials with low SR and cost. RMs are notable for their stator windings configurations; SRMs have concentrated windings whereas SynRMs have distributed windings. Both RM types are easier to cool than PMSMs or IMs because the rotor does not have PMs or windings. All the developed torque in RMs is generated from the magnetic reluctance of stacking electric steel plates with a particular geometry consisting of

flux barriers (holes) and segments structurally constrained within the rotor.

While some view magnet-free traction motors as a promising research direction, PMSMs, and PMa-SynRMs with REPMs are, at present, the most attractive motors for an EV. This is true because they have the highest power density and efficiency among the mentioned topologies. Their main drawbacks are cost and reliance on PMs. In a fair apples-to-apples comparison, it has been reported that PMa-SynRMs should have a smaller reliance on REEs whereas PMSMs should have a better performance in terms of power-density and efficiency [9].

Given these strategies that consider the SR of critical materials, a new strategy can be developed by using optimization-based design methodology. This methodology is comprised of detailed analysis calculations, the chosen objective functions, and the use of an optimization engine. Firstly, the detailed analysis is constructed from various models found in the literature and integrates large amounts of data and processes to propose a motor design. To decrease complexity in describing the design model, the detailed design calculations consider only surface-mounted PMSMs. However, this methodology can be adapted to other topologies and motor types. Secondly, the electric traction motors (and other technologies) may be designed to minimize the mass of materials by using their corresponding SRs scores as weighing factors. This will provide the advantage of optimizing for product transferred SR which can find non-dominated solutions among competing materials and component masses, rather than optimizing for a specific component a priori (e.g., minimizing REPM mass). The three objectives for this design methodology are to minimize motor mass, energy consumption, and motor SR-equivalent (the new proposed objective). Finally, the optimization engine is a tool to search for feasible and non-dominated solutions within the design space. In this case, a genetic algorithm (GA) is used. The following section will detail much more about the calculations and steps in the optimization-based design methodology.

III. MOTOR OPTIMIZATION-BASED DESIGN MODEL
Fig. 1 shows the design framework for electric traction motors, which is adapted from Cassimere and Sudhoff [12], Cassimere et al. [13], and Sudhoff [14]. This framework is applied to EVs with an electric motor topology of a surface-mounted PMSM. The general approach used here could be applied to other PMSM types such as an interior permanent magnet machine. Indeed, the design method set forth in [15] could be adapted to this end. However, in order to keep focus, studies here are limited to surface-mounted machines. The description of this framework will start with the design space and move to detailed analysis, then objective functions, and finally, to the optimization engine.

A. DESIGN SPACE
The design space (or search space) is composed of fixed and variable design parameters. The fixed parameters constitute
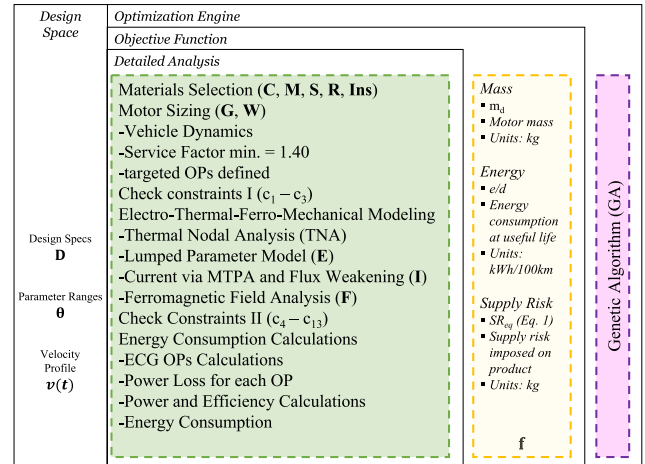

FIGURE 1. Design framework for electric traction motors.

the design specifications, $\mathbf{D}$, i.e., the coefficients, assumptions, and specifications that are used in the design model (see Table S2 in the SI). The variable parameters are managed separately from the fixed parameters; the ranges for the variable parameters are defined by θ, which provides a delimited continuous range or allowable discrete values for each variable parameter (see Table S3). An additional variable to be considered during design is the velocity profile, $v(t)$, which is obtained from the specified drive cycle (see Fig. S1a). The velocity profile is used in the sizing of motors and calculating vehicle energy consumption. The drive cycle may change over time due to human behavior, weather, transportation ecosystem, etc.

B. DETAILED ANALYSIS
The first step of the detailed analysis is materials selection. For each component, allowable material types (e.g., list of material grades) are specified by the following variables: conductor windings $\mathbf{C}$, permanent magnets $\mathbf{M}$, stator laminations $\mathbf{S}$, rotor laminations $\mathbf{R}$, and thermal insulation $\mathbf{Ins}$. Associated with each material type are all the material properties needed to complete the design (see Table S4-S11 in SI). Table 1 presents a summary of the motor parts with a simplified description of the material requirements [16], [17].

The next step is to determine the motor size according to the design specifications. The 2019 Nissan Leaf S EV will be used as an example (see Table 2) [18]. The EV coefficients considered in the design model are 0.0083 rolling resistance, 0.28 aerodynamic drag, 96% transmission efficiency, and 7.5 mph headwind air velocity. These EV system properties are important, because when the design of the motor is changed, the mass of the motor may be reduced. This may result in secondary mass savings (SMS).[1] We have assumed that SMS is 0.95 kg for every 1 kg of primary mass saved in

---

[1]When less material mass is required for the structural support of a component because the mass of the component has been reduced, this is termed secondary mass savings (SMS).

TABLE 1. Summary of motor parts with description and materials considered.

Part	Materials	Function
Stator and Rotor -Laminations -Coating	-M19, M36, M43, M47 -phenolic resin	-Hold the conductors or PMs in the slots -Decreases Eddy current losses
Magnet wires -Conductors -Enamel	-Al, Cu -polyester resin	-electric-to-magnetic energy conversion -electrical insulation
Permanent magnets -Magnet -Coating	-sintered Nd-Fe-B, Sm-Co -Ni for Nd-Fe-B	-Magnetomotive force source that follows an opposite pole of the rotating magnetic field induced by stator windings. -Prevents corrosion
Stator Insulation System -Slot liner and separator foils -Phase to phase insulation tape -Impregnation -Phase conductor insulation -Lacing cord	-polyethylene terephthalate -mica tape -epoxy resin -silicone -Nylon 6	-Prevents a short circuit between coils and stator in slot -coils with different phases -vibration protection; increase thermal conduction for proper cooling -Used in wire terminals to reach electrical and mechanical conditions at high temperatures -Tightens or packs end-windings
Rotor fastening -Rotor endplates -Magnet fixation resin	-Stainless steel -Methacrylate ester resin	-Fast the endbells to housing -Adhere magnets to rotor
Housing -Housing body -Endbells	-Aluminum -Paint/varnish -Aluminum -Paint/varnish	-Encloses the motor -Prevents corrosion; increases thermal conduction -Encloses the motor -Prevents corrosion; increases thermal conduction
Shaft	Low-alloy medium carbon steel	Transmits torque to powertrain
Bearings	Low-alloy medium carbon steel	Mounts the shaft
Resolver	Laminations, wire magnet, etc.	Measures rotor position and speed
Terminal block frame	Polybutylene terephthalate	Connects cables from inverter and from windings
Fasteners and plate	-Low-alloy medium carbon steel -Zinc (galvanization)	-Holds the motor frame -Prevents corrosion
Connector lugs	Copper	Connects end-wiring with PBT terminal

comparison to the actual motor of the case study EV [19]. The Nissan motor has a continuous power and torque of 110kW and 320N-m (peak power and torque are 150kW and 436 N-m), and a constant power speed range from 3283 rpm to 9795 rpm [18], [20], [21]. Given an initial 3 cm shaft radius and the other parameters as denoted by θ, the motor

dimensions and volumes of the rotor and stator cores, the PMs, and slot liners are calculated and stored in the geometry vector **G**. Later, we will use an iterative process to converge to the final shaft radius. The windings vector **W** includes their symmetric distribution, the number of conductors per slot, the end windings design, and the total volume. With these calculations and the mass estimates of other inactive motor components, the motor mass is calculated [16], [17]. Once the mass calculations are complete, the EV mass is updated according to the defined SMS. Finally, the motor sizing step calculates the tractive force (Fig. S1b), torque (Fig. S1c), and power (Fig. S1d) profiles, the rated and maximum torque and power, the base and maximum speeds, and the power and torque versus speed characteristic curves (i.e., continuous and intermittent) (see Fig. 2a-b), as modeled by Akl and others [21]. Based on the required peak torque, the shaft radius is recalculated. For more details on motor sizing, refer to Pseudocode S1 from the SI.

TABLE 2. 2019 Nissan Leaf S EV Specifications.

EV Specifications	Symbol	Value	Units
Gross vehicle mass	GVM	1990	kg
Curb vehicle mass	CVM	1558	kg
Motor mass	m_d	58	kg
Maximum velocity	V_{vx}	89.5	m/s
Maximum acceleration	dV_{vx}/dt	60 / 7.5	mph
Gradeability at V_{vx}	α	6.35	%
Wheel radius	r	0.3178	m
Distance for one charge		270	km
Transmission ratio	k_g	8.1938	-
Effective frontal area	A_v	2.1465	m^2
Axle moment of inertia	J_{axle}	3	kg/m^2

After sizing the motor, the targeted operating points (OPs) are selected as shown in Fig. 2b and Pseudocode S2. The targeted OPs are those for which the constraints will be evaluated. Three additional constraints can also be checked at this stage. These are the tooth aspect ratio (ratio less than 10), the slot opening factor (less than 1.5), and a mass constraint (mass less than 65 kg). When a constraint is violated during the process, there is no point in evaluating the remaining constraints (this iteration is terminated); this serves to reduce the optimization run time. The program then checks the constraints are implemented based on the literature [12], [14]. The number of constraints must be known a priori to determine if the design satisfies all constraints. The number of constraints is as follows:

$$N_C = n_{OP-I} + n_{C \; per \; OP} \, n_{OP}^* \tag{1}$$

where n_{OP-I} is the number of OP-independent constraints, $n_{C per \; OP}$ is the number of constraints per OP, and n_{OP}^* is the number of OPs. The structure of the constraint formulations are such so that when the jth constraint c_j is satisfied its numerical value is 1; otherwise, it takes on a value between 0 and 1 (see SI). An unsatisfied constraint closer to 1 means that the constraint is closer to being satisfied.

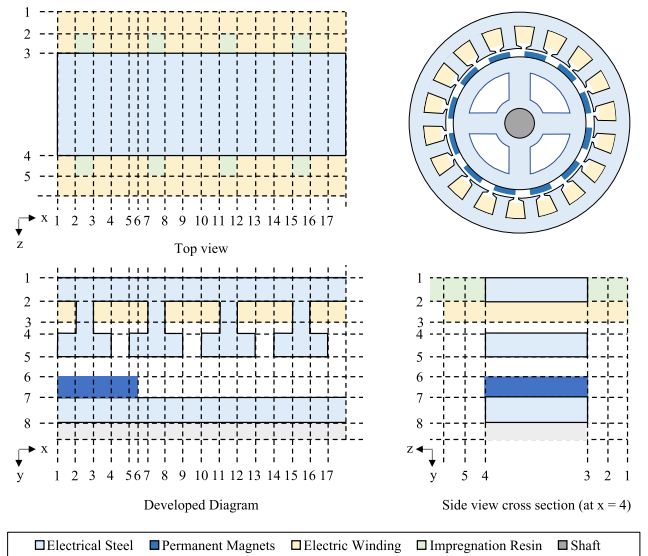Once these constraints are satisfied, the electrical, ferromagnetic, mechanical, and thermal parameters are calculated
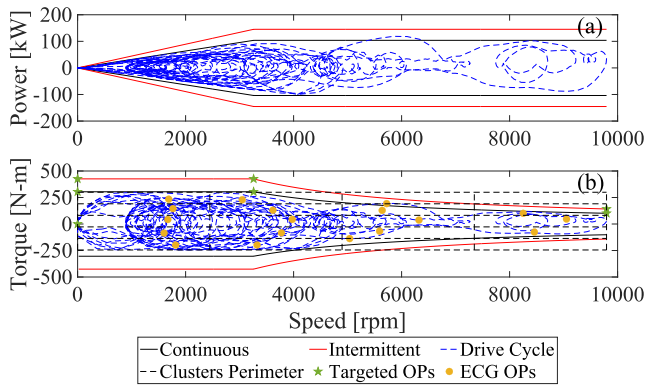
FIGURE 2. Motor (a) power versus speed characteristic curves, and (b) torque versus speed characteristic curves.

alone are that the maximum current density may not correspond with the maximum peak temperature on the windings (since the role of geometry on heat transfer is not considered) and that it ignores the permissible magnet peak temperature. A TNA estimates the conductance of each cuboid element, its interaction with neighbor elements, and how heat is removed from the windings and the permanent magnets. However, the main drawback for TNA is that it takes longer to estimate the temperature profile than to calculate the current density.

FIGURE 3. Developed diagram including top and side views of a surface-mounted PMSM (inactive components, motor frame, and jacketed heat removal system not shown).

for each targeted OP (see Pseudocode S3 in SI). Before these calculations take place, a thermal nodal analysis (TNA) is done using the OP-independent calculations (Pseudocode S5). The purpose of the TNA is to model the temperature profile of a representative motor region that includes the stator and rotor electrical steel laminations, PMs, electrical windings, impregnation resin between motor frame and end windings, air gap, and shaft as shown in Fig. 3. This region represents $2\pi/P$ of a revolution for surface-mounted PMSM, where P is the number of poles contained in that motor. For image clarity, the figure shows four slots per pole, but in reality, the model will have six slots per pole (i.e., the motor has three-phases and the number of slots per pole per phase is fixed at 2). Since the winding distribution is symmetric, the temperature profile is assumed to be the same across any motor region. The TNA creates a thermal equivalent circuit (TEC) of cuboid elements bounded by the grid shown in Fig. 3. Solid-to-solid neighbors have thermal conductance heat transfer while solid-to-air elements have a convective heat transfer. After the initial TNA, the previously mentioned parameters are calculated for the first targeted OP. Subsequently, the rest of the OP-dependent heat transfer calculations are completed (Pseudocode S6). Then, following the calculation of electrical parameters **E** and **I**, the ferromagnetic parameter **F**, the torque as a mechanical parameter T_{ec}, and temperature profile and other thermal parameters **Th** (Pseudocode S7-S9), an iterative process (see Fig. 1) is conducted until convergence on the temperature profile is achieved. If all constraints for this first OP are satisfied, the same procedure is followed for the next OP. If for any OP, some of the constraints are not satisfied, then the code stops and starts over with a new θ vector. If all constraints for all targeted OPs are satisfied, a feasible motor design is found.

Some preliminary design methods use the maximum current density (i.e., maximum current divided by the bare conductor cross-sectional area) as an implicit metric for maximum temperature on the windings. However, this method may not be as accurate as conducting a TNA or equivalent method. Two major drawbacks of considering current density

To summarize, for a given set of parameters an iterative process is used to obtain temperature convergence. The rest of the constraints for this specific OP are checked. If they are satisfied, then the loop continues to the next targeted OP. If all constraints are satisfied, then a feasible solution is found. The final steps are related to the calculation of the energy consumption over the useful life of the product.

The data used to predict the energy consumption throughout the EV useful life was obtained from the Worldwide harmonized Light vehicle Test Procedure (WLTP) for a class 3 vehicle for a typical global driver characteristic [22], [23], [24]. This drive cycle was adapted to match the EV specifications for its maximum velocity and acceleration, as shown in Table 2. 2019 Nissan Leaf S EV Specifications. A vehicle dynamics model was used to determine the traction force for the driving cycle [17], [21]. The model results can then be visualized with the torque versus speed diagram (as in Fig. 2b). To determine the representative OPs from the drive cycle, the energy center of gravity (ECG) was used [25]. The torque-speed diagram is divided into clusters, and the ECG are localized and estimated for each cluster. In this paper, these are termed the ECG OPs (see Fig. 2b). Once they are localized, the targeted OP process calculations are repeated. There is no need to check constraints because

the targeted OPs have already been verified. These targeted OPs are located on the operating region boundary, while the ECG OPs lie within the region. Thus, the constraints for the ECG OPs need not be checked. Using the results from this analysis, power and efficiency calculations are obtained, and the energy consumption along the useful life of the product is calculated in terms of kWh/100km (Pseudocode S4).

C. OBJECTIVE FUNCTIONS

As discussed in the previous subsection, the detailed analysis contains all the calculations needed to evaluate the objective functions. In this case, it is desired to minimize three performance measures: 1) motor mass, 2) energy consumption, and 3) SR-eq. score (equivalent supply risk). Reducing the motor mass will result in energy savings, as well as SMS throughout the rest of the system (i.e., EV) which may result in additional energy savings [19], [26]. Minimizing energy consumption will mean lower energy costs, but also provide environmental benefits, which is an important variable to consider [17], [27]. Lowering the SR-eq. will reduce the masses of the critical materials in the motor from the most to the least critical. The proposed SR-eq. is a new metric that when optimized reduces future supply disruptions associated with the manufacturing sector by reducing the material demands of a product. An increased SR-eq. may lead to price volatility and component/product shortages and deleteriously impact the consumer.

According to the latest USGS review and revision of non-fuel mineral list, fifty materials are considered critical for the United States. A selected list is shown in Table S1 (please refer to the SI). Their quantitative assessment for defining SR for one commodity is based on three factors: the potential of a foreign supply disruption, the dependency of the targeted country manufacturing sector on trade exposure with foreign supply, and the economic vulnerability of the targeted country manufacturing sector to a supply disruption. The geometric mean of these three factors gives a SR score. Some minerals were assessed qualitatively because of either a lack of available data or the mineral has a domestic single point of failure (i.e., there is a single domestic producer in the country of interest). For more details about the SR scoring model, please refer to the work done by Nassar and Fortier [10].

Now, the SRs associated with single commodities in a targeted country, in this case the United States, can be used in combination with the material masses in a product for calculating an SR score for a product. The proposed score can be calculated as a weighted mean formula, as follows:

$$SR_{eq} = \frac{\sum_{i=1}^{n} m_{mfg,i} R_i}{\sum_{i=1}^{n} m_{mfg,i}} = \frac{\sum_{i=1}^{n} s_i m_i SR_i}{\sum_{i=1}^{n} s_i m_i} \quad (2)$$

where n is the number of materials contained in the product, where the product, which may consist of multiple components, has multiple materials. For example, an REPM is made from multiple material types. In (2), s_i is the ratio of the mass required to manufacture a product or component divided by the final mass of the component for the ith material

(usually, $s_i > 1$; this is the so-called buy-to-fly ratio), m_i is the mass of ith material in the product, and SR_i is the supply risk of the ith material. The sum of mass of all materials in the product is denoted as the design mass m_d. Note that $m_{mfg,i}$ is the mass required for ith material to produce one product and is equal to $s_i m_i$. The variable m_i can be calculated from the product geometry. The variables s_i can be found from life cycle inventories and other studies in the literature and SR_i may be found in government reports or may be calculated for other targeted countries as explained earlier. Since the scope of this study does not consider any manufacturing data, to use (2), s_i will be assumed to equal 1 for all i. The SR_{eq} represents a weighted mean, where the weights are the masses required for each material and the data elements are the supply risk scores, and thus has no units. Scores may range from the lowest to the highest SR_i score of materials contained in the product. SR_{eq} may be minimized by minimizing the mass of specific materials and/or selecting material types that have smaller supply risks.

D. OPTIMIZATION ENGINE

Different population-based optimization techniques have been applied to electric motor design [12], [28], [29], [30], [31]. Their applications have proven to be useful due to their high dimensional search space capabilities, which is convenient for solving complex problems such as electric motor design. For this paper, a genetic algorithm (GA), i.e., the Genetic Optimization Systems Engineering Tool (GOSET) – version 2.6, was applied to the described design. The GOSET algorithm includes the canonical mechanisms of GAs (selection, crossover, and mutation) and other operators found in the literature (elitism, migration, random search, diversity control, scaling, and death). For more details, refer to the GOSET documentation [32]. Table S3 from the SI includes all 27 genes and the ranges considered. It is important to state that the selection of other genes and ranges can result in different outcomes. The fitness function is a vector that contains the three objective functions:

$$\mathbf{f} = [m_d \ e/d \ SR_{eq}]^T \quad (3)$$

where m_d is the designed motor mass, e/d is the energy consumption per unit of distance across the useful life, and SR_{eq} is the SR-eq. score. This fitness function is used to find feasible solutions. The non-dominated solutions will be plotted as a Pareto front. The solutions lying on the front are considered optimal.

To achieve this, a GA is set to run a population size of 3,000 and will run for 2,000 generations. Two different magnets for the motor design are considered: Sm-Co magnets and sintered Nd-Fe-B magnets. The results display a matrix of plots where the ith row and jth column ($i \neq j$) plot present the Pareto front for the ith and jth objective functions. The plots on the diagonal ($i = j$) show a frequency histogram of values for ith objective function for the last generation of the non-dominated solutions. In addition, the parameters distribution will show how they relate to the non-dominated solutions.
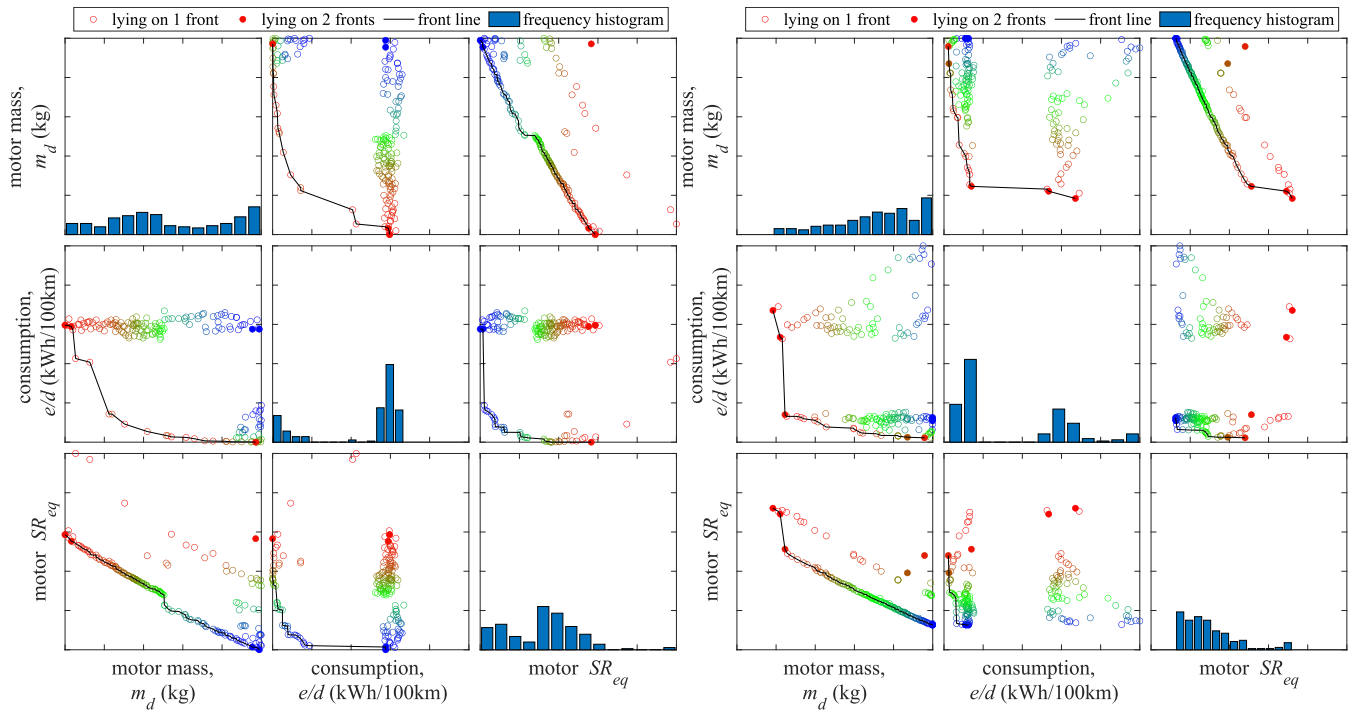
FIGURE 4. Pareto fronts for all objective function pairs and density histograms for each objective function (left: Sm-Co, right: Nd-Fe-B).
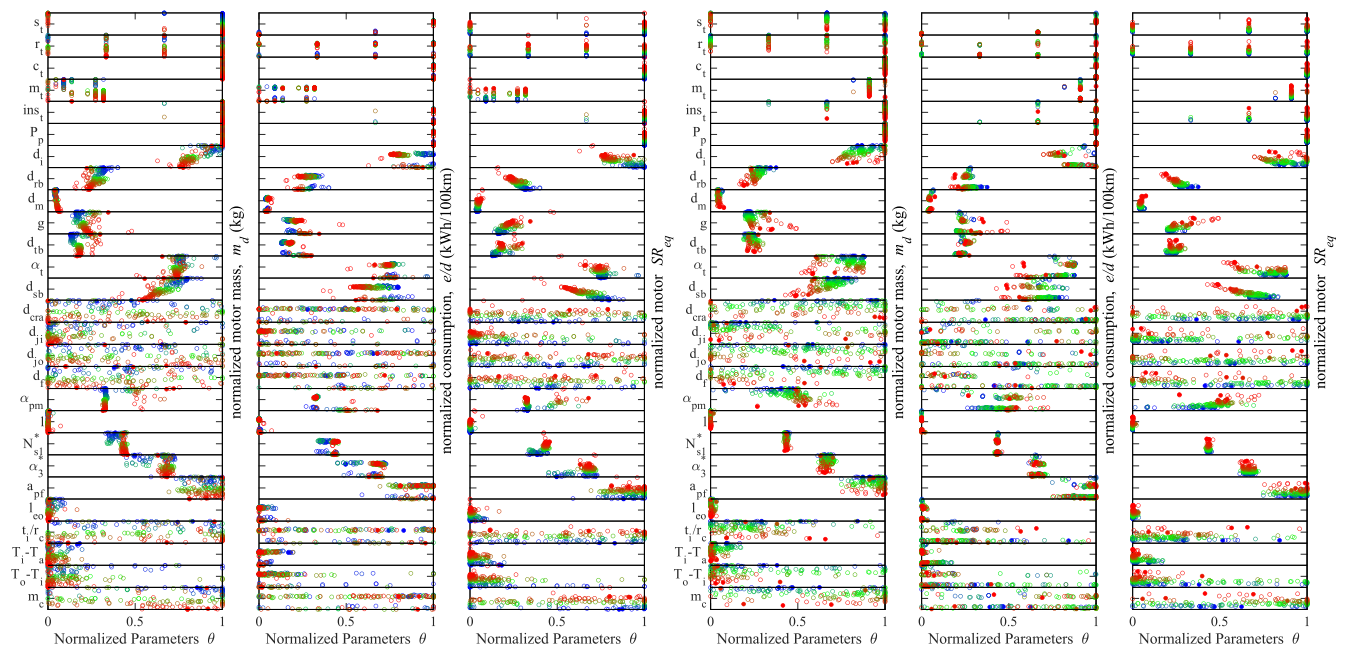

FIGURE 5. Normalized parameter distributions (left: Sm-Co, right: Nd-Fe-B).

The data points are colored in a rainbow fashion so that each color corresponds to a non-dominated solution lying on the Pareto fronts. The colors are consistently sorted in ascending form in terms of motor SR-eq. (blue = lowest,

and red = highest) across all figures shown in this study. The results will be analyzed and discussed, specifically regarding the benefits of the SR-eq. score, the design model, and future improvements.
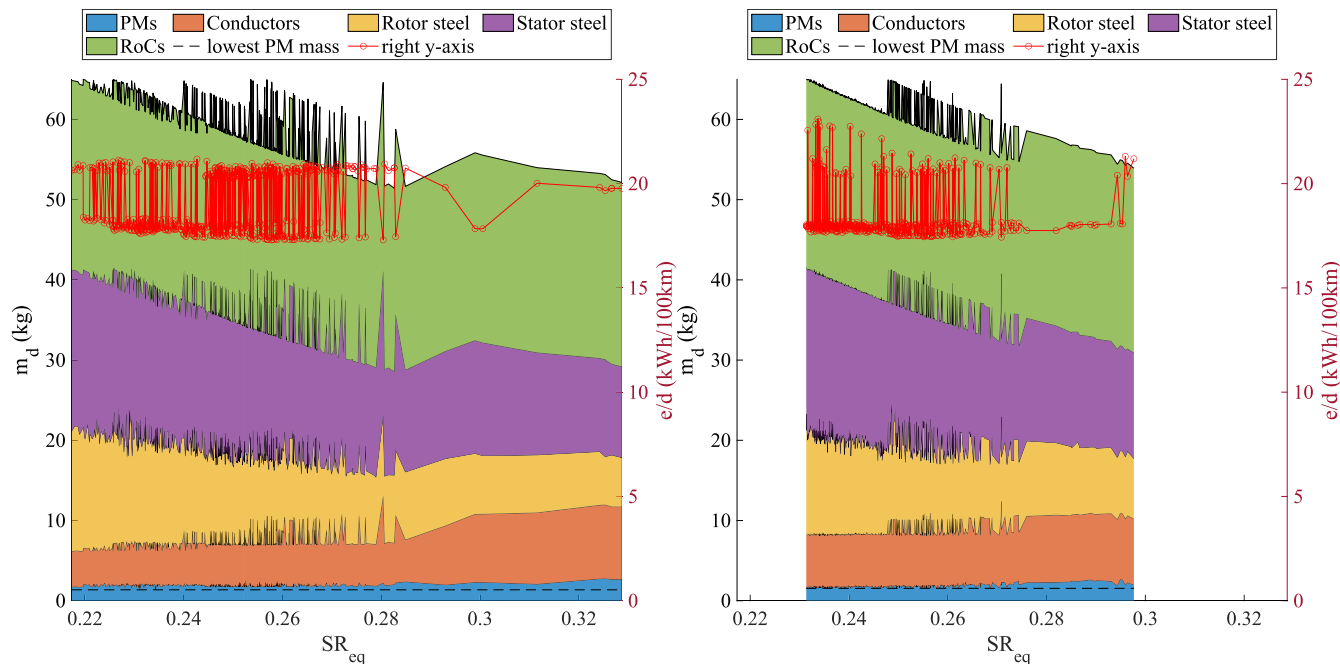
FIGURE 6. The effect of mass composition of main components and rest of components (RoCs) on the three objective functions (left: Sm-Co, right: Nd-Fe-B).

IV. RESULTS AND DISCUSSION

Fig. 4 shows the final Pareto fronts for the non-dominated solutions. These points are displayed for each objective function pair and frequency histograms for each objective function are also shown. Graphs are presented for both magnet types: Sm-Co and Nd-Fe-B. The relationships among the objectives for both magnet types are similar. It is important to note that for each pair of objectives the three-dimensional Pareto front is projected onto a plane pair (e.g., objective 1 vs. objective 2). The open and closed points represent those non-dominated solutions lying on 1 and 2 Pareto front projections, respectively. It is important to specify that there were more non-dominated solutions not plotted in the figure. The reason behind not plotting them is because it would be more difficult to visualize the results. Those eliminated non-dominated solutions are the ones not lying on any of the Pareto front projections. Each axis of each plot is delimited and normalized from minimum value (equal to 0) to maximum value (equal to 1). This figure may be proposed to show the results for multi-objective optimization problems.

In the mass vs SR-eq. graphs of Fig. 4 (for both Sm-Co and Nd-Fe-B), there are points that align to form multiple sets (traces) of solutions; along a trace the decision variables change, and each trace is likely associated with a different material. Regardless, all these points are non-dominated solutions. Also evident in the figure is that there is a tradeoff between motor mass and energy consumption per unit of distance (i.e., the lighter the motor, the worse it performs). The motor mass and SR-eq. have an inverse relationship because of the way SR-eq. Finally, the energy consumption

and SR-eq. score also have a tradeoff for motors with high mass. Further analysis on the variable and other parameters distributions is needed to understand these phenomena, especially, the effect of SR-eq.

In Fig. 4, when comparing from one magnet type to the other, since Sm-Co magnets have a smaller SR-eq. than the Nd-Fe-B magnets, the SR-eq. for motors (PMSMs) made with these magnets have similar behavior. Also, one can observe that PMSMs with Sm-Co perform better in terms of motor mass and energy consumption. This observation has been reported in the literature and may be due to multiple factors despite Nd-Fe-B magnets having a higher maximum energy density than Sm-Co [33]. These factors may include the remanent flux density and thermal resistance to demagnetization.

To explore how changes in the parameters in θ affect the three objective functions, Fig. 5 was prepared. Six rectangular boxes are shown (3 objectives × 2 magnet types), and each box consists of 27 rectangles (one for each parameter). Each rectangle displays the non-dominated points; the horizontal position of each point is the normalized parameter value for that variable and the vertical position is the objective function value. The color for the displayed points follows the convention established previously. Each point shown in Fig. 4, is displayed in Fig. 5 for the corresponding parameter value.

In Fig. 5, the first six variables are dependent on the material types selected. Almost all designs use stator steel type s_t corresponding to M47, followed by a few designs with M43 and M19. There is more flexibility in selecting

the rotor steel type r_t than the stator. The conductor type c_t for these runs tend to correspond to aluminum. The material type m_t used varies among three to seven different grades for each Sm-Co and Nd-Fe-B run. Most designs use the thermal insulation classification corresponding to the N NEMA class (200° maximum operating temperature), followed by the H NEMA class (180° maximum operating temperature). The thermal insulation class may be decreased to a lower grade depending on the heat transfer configuration (e.g., a jacketed motor frame with water) and changes to improve materials to increase conductance (e.g., impregnation resins between end windings and motor frame).

Regarding the l, the peak fundamental conductor density N_{s1}^*, the third harmonic conductor density α_3^*, the conductors packing factor a_{pf}, and the end winding offset l_{eo} have a relatively well defined range that make feasible motor designs. The rest of the geometric/winding parameters, the depth of inert region d_i, the depth of rotor backiron d_{rb}, the depth of tooth base d_{tb}, the depth of magnet d_m, the air gap g, the tooth fraction α_t, the depth of stator backiron d_{sb}, the magnet fraction α_{pm}, the active (or stack) length geometric/winding parameters show no correlation to any of the objectives. The only observed correlation with energy performance is the stator steel selection (less energy consumption for M43 or M19).

In addition to the effect of changes in the parameters above on objective function values, the motor outer diameter-to-active length ratio $2r_{ss}/l$ may be an important factor to consider. For Sm-Co, this ratio ranges from 2.4 to 4.5 whereas for Nd-Fe-B it ranges from 3.6 to 4.6. The SI shows the $2r_{ss}/l$ distribution for all three objective functions (see Fig. S2). However, there is no clear indication that $2r_{ss}/l$ and the objective functions are related for the non-dominated solutions.

According to how SR-eq. was defined, one may observe an inverse linear relationship between motor mass and the SR-eq. The effect of minimizing for SR-eq. is that for a given motor mass, the materials masses experiencing a high SR tend to be exchanged for material masses with a low SR. This is an important observation and reveals that using SR-eq. as a design strategy is different than minimizing mass. In order to better visualize this observation, see Fig. 6. This figure shows the effect of mass composition of the main components (stator, rotor, conductor windings, and PMs) and the agglomeration of the rest of components (RoCs) on all three objective functions for all non-dominated design solutions. For a complete visualization, please refer to Fig. S3 and S4 from the SI. As seen in the SI, those disturbances shown in the mass of components sorted by increasing SR-eq. are due to discrete parameters (e.g., stator material selection). It is seen that the PMs and conductors (in terms of mass) do not vary as much as the stator and rotor masses. Another observation is that the overall motor mass is more sensitive to rotor and stator component masses. Finally, among the components listed, the PMs and conductors are the ones experiencing highest SRs (SRs for Sm-Co is 0.43, for Nd-Fe-B is 0.24-0.26, and aluminum conductors are 0.60).

This Fig. 6 shows that the reduction in SR-eq. scores is aligned to those design solutions with reduced PMs and windings mass. However, despite these solutions reached a reduced mass of PMs and conductors, the overall motors have increased mass. This proves that minimizing for mass is not necessarily an appropriate measure of minimizing the mass of components experiencing high SR. Therefore, optimizing for a lighter motor is not the same as optimizing for reduced SR-eq.

The design code used for the design of the electric machine is mature and found to be quite accurate. In particular, finite element analysis (FEA) validation of the design code is given in [34], [35], and [36]. Generally, there is no guarantee that a GA will identify the optimal solution(s). However, the quality of solutions can be tracked during the GA procedure to assess whether the algorithm is converging. In the present research, the median, mean, and best fitness for each generation were graphed to visually determine if the run was converging (i.e., the best fitness for each objective function approaches a constant as the number of generations increases), as explained by Sudhoff [14] (see Fig. S5). Another way to judge the quality of the solution is to see how close the solution is to some of the design constraints (optimal solutions often occur on constraints). For example, Fig. S6 shows that for the non-dominated solutions, the largest calculated values of each ferromagnetic constraint, across all the targeted OPs, are very close to the constraint limits. These constraints serve to limit the search for other motor solutions, which are not feasible.

V. SUMMARY AND CONCLUSION

Electric traction motors are a critical component in the new generations of EVs. In this study, a new design framework has been proposed to address the SR issues of increasing demands for critical materials such as neodymium. A design model for electric traction motors was proposed and used to optimize motor mass, energy consumption, and SR-equivalent. To our knowledge, this is the first paper that proposes a general function for minimizing the supply risk (SR) for all critical materials and a method for addressing this issue at the engineering design stage.

For the non-dominated solutions obtained with our method, we examined the relationship among objectives and variable parameters. Minimizing the SR-eq. proved to be useful, because it reached the goal of minimizing for those materials experiencing the highest SRs in order of priority. It was seen that minimizing for a lighter motor is not the same as minimizing the SR. This method for minimizing the SR-eq. can be applied to other applications or products. Applying this special consideration may help decrease the risks associated with the supply of these critical materials. Also, instead of targeting a specific material, the proposed method may consider the system complexity to minimize the SRs of all materials needed. Directions for future work with this optimization-based model may include adding more motor topologies and exploring new objective functions, e.g., minimizing motor cost or lifecycle environmental impact.

As a final thought, the proposed SR-eq. can be another design strategy that seeks to reduce future supply disruptions for the manufacturing sector that may lead to price volatility and product shortages and deleteriously impact the consumer. In the case of green energy technologies, these disruptions also interrupt our efforts to work toward a more sustainable and cleaner future.

ACKNOWLEDGMENT

REFERENCES

[1] United Nations. (2022). *The Sustainable Development Goals Report 2022*. Accessed: Dec. 8, 2022. [Online]. Available: https://unstats.un.org/sdgs/report/2022/The-Sustainable-Development-Goals-Report-2022.pdf

[2] D. Bauer, D. Diamond, J. Li, D. Sandalow, P. Telleen, and B. Wanner, "U.S. Department of Energy critical materials strategy," United States Dept. Energy, Tech. Rep., Dec. 2010, doi: 10.2172/1000846.

[3] N. T. Nassar et al., "Evaluating the mineral commodity supply risk of the U.S. manufacturing sector," *Sci. Adv.*, vol. 6, no. 8, 2020, Art. no. eaay8647, doi: 10.1126/sciadv.aay8647.

[4] USGS. *U.S. Geological Survey Releases 2022 List of Critical Minerals*. Accessed: Feb. 21, 2022. [Online]. Available: https://www.usgs.gov/news/national-news-release/us-geological-survey-releases-2022-list-critical-minerals

[5] T. E. Graedel et al., "Methodology of metal criticality determination," *Environ. Sci. Technol.*, vol. 46, no. 2, pp. 1063–1070, Jan. 2012, doi: 10.1021/es203534z.

[6] T. Igogo, D. Sandor, A. Mayyas, and J. Engel-Cox. (Aug. 2019). *Supply Chain of Raw Materials Used in the Manufacturing of Light-Duty Vehicle Lithium-Ion Batteries*. [Online]. Available: https://www.nrel.gov/docs/fy19osti/73374.pdf

[7] J. M. D. Coey, "Perspective and prospects for rare Earth permanent magnets," *Engineering*, vol. 6, no. 2, pp. 119–131, 2020, doi: 10.1016/j.eng.2018.11.034.

[8] J. Cui et al., "Manufacturing processes for permanent magnets: Part I—Sintering and casting," *Jom*, vol. 74, no. 4, pp. 1279–1295, 2022, doi: 10.1007/s11837-022-05156-9.

[9] P. Ramesh and N. C. Lenin, "High power density electrical machines for electric vehicles—Comprehensive review based on material technology," *IEEE Trans. Magn.*, vol. 55, no. 11, pp. 1–21, Nov. 2019, doi: 10.1109/TMAG.2019.2929145.

[10] N. T. Nassar and S. M. Fortier, "Methodology and technical input for the 2021 review and revision of the U.S. Critical Minerals List," United States Geol. Surv., Reston, VA, USA, Open-File Rep. 2021–1045, 2021, doi: 10.3133/ofr20211045.

[11] J. Cui et al., "Current progress and future challenges in rare-Earth-free permanent magnets," *Acta Mater.*, vol. 158, pp. 118–137, Oct. 2018, doi: 10.1016/j.actamat.2018.07.049.

[12] B. N. Cassimere and S. D. Sudhoff, "Population-based design of surface-mounted permanent-magnet synchronous machines," *IEEE Trans. Energy Convers.*, vol. 24, no. 2, pp. 338–346, Jun. 2009, doi: 10.1109/TEC.2009.2016150.

[13] B. N. Cassimere, S. D. Sudhoff, and D. H. Sudhoff, "Analytical design model for surface-mounted permanent-magnet synchronous machines," *IEEE Trans. Energy Convers.*, vol. 24, no. 2, pp. 347–357, Jun. 2009, doi: 10.1109/TEC.2009.2016139.

[14] S. D. Sudhoff, *Power Magnetic Devices: A Multi-Objective Approach*, 2nd ed. Hoboken, NJ, USA: Wiley, 2022.

[15] R. Lin, S. D. Sudhoff, and V. C. D. Nascimento, "A multi-physics design method for V-shape interior permanent-magnet machines based on multi-objective optimization," *IEEE Trans. Energy Convers.*, vol. 35, no. 2, pp. 651–661, Jun. 2020, doi: 10.1109/TEC.2019.2958928.

[16] A. Nordelöf, E. Grunditz, A. M. Tillman, T. Thiringer, and M. Alatalo, "A scalable life cycle inventory of an electrical automotive traction machine-Part I: Design and composition," *Int. J. Life Cycle Assessment*, vol. 23, no. 1, pp. 55–69, 2018, doi: 10.1007/s11367-017-1308-9.

[17] A. Nordelöf, E. Grunditz, S. Lundmark, A. M. Tillman, M. Alatalo, and T. Thiringer, "Life cycle assessment of permanent magnet electric traction motors," *Transp. Res. D, Transp. Environ.*, vol. 67, pp. 263–274, Feb. 2019, doi: 10.1016/j.trd.2018.11.004.

[18] EVSpecifications. *Nissan Leaf S—Specifications and Price*. Accessed: Aug. 8, 2022. [Online]. Available: https://www.evspecifications.com/en/model/2bc417

[19] E. Alonso, T. M. Lee, C. Bjelkengren, R. Roth, and R. E. Kirchain, "Evaluating the potential for secondary mass savings in vehicle lightweighting," *Environ. Sci. Technol.*, vol. 46, no. 5, pp. 2893–2901, 2012, doi: 10.1021/es202938m.

[20] EV Database. *Nissan Leaf*. Accessed: Aug. 8, 2022. [Online]. Available: https://ev-database.org/car/1656/Nissan-Leaf

[21] M. M. Akl, A. A. Ahmed, and E. E. M. Rashad, "A wide component sizing and performance assessment of electric drivetrains for electric vehicles," in *Proc. 21st Int. Middle East Power Syst. Conf. (MEPCON)*, Dec. 2019, pp. 834–839, doi: 10.1109/MEPCON47431.2019.9008195.

[22] B. Ciuffo et al., "Development of the worldwide harmonized test procedure for light-duty vehicles pathway for implementation in European Union Legislation," *Transp. Res. Rec.*, vol. 2503, no. 1, pp. 110–118, 2015, doi: 10.3141/2503-12.

[23] L. Mao, A. Fotouhi, N. Shateri, and N. Ewin, "A multi-mode electric vehicle range estimator based on driving pattern recognition," *Proc. Inst. Mech. Eng., C, J. Mech. Eng. Sci.*, vol. 236, no. 6, pp. 2677–2697, 2022, doi: 10.1177/09544062211032994.

[24] M. De Santis, L. Silvestri, and A. Forcina, "Promoting electric vehicle demand in Europe: Design of innovative electricity consumption simulator and subsidy strategies based on well-to-wheel analysis," *Energy Convers. Manag.*, vol. 270, Oct. 2022, Art. no. 116279, doi: 10.1016/j.enconman.2022.116279.

[25] S. Pastellides, S. Gerber, R. J. Wang, and M. Kamper, "Evaluation of drive cycle-based traction motor design strategies using gradient optimisation," *Energies*, vol. 15, no. 3, p. 1095, Feb. 2022, doi: 10.3390/en15031095.

[26] T. Hottle, C. Caffrey, J. McDonald, and R. Dodder, "Critical factors affecting life cycle assessments of material choice for vehicle mass reduction," *Transp. Res. D, Transp. Environ.*, vol. 56, pp. 241–257, Oct. 2017, doi: 10.1016/j.trd.2017.08.010.

[27] A. Rassõlkin et al., "Life cycle analysis of electrical motor-drive system based on electrical machine type," *Proc. Estonian Acad. Sci.*, vol. 69, no. 2, p. 162, 2020, doi: 10.3176/proc.2020.2.07.

[28] M. L. Bash and S. Pekarek, "Analysis and validation of a population-based design of a wound-rotor synchronous machine," *IEEE Trans. Energy Convers.*, vol. 27, no. 3, pp. 603–614, Sep. 2012, doi: 10.1109/TEC.2012.2203136.

[29] M. L. Bash and S. D. Pekarek, "Modeling of salient-pole wound-rotor synchronous machines for population-based design," *IEEE Trans. Energy Convers.*, vol. 26, no. 2, pp. 381–392, Jun. 2011, doi: 10.1109/TEC.2011.2105874.

[30] T. Tušar, P. Korošec, G. Papa, B. Filipiè, and J. Šilc, "A comparative study of stochastic optimization methods in electric motor design," *Appl. Intell.*, vol. 27, no. 2, pp. 101–111, Aug. 2007, doi: 10.1007/s10489-006-0022-2.

[31] M. E. Beniakar, P. E. Kakosimos, and A. G. Kladas, "Strength Pareto evolutionary optimization of an in-wheel PM motor with unequal teeth for electric traction," *IEEE Trans. Magn.*, vol. 51, no. 3, pp. 1–4, Mar. 2015, doi: 10.1109/TMAG.2014.2347963.

[32] S. D. Sudhoff, "GOSET: Genetic optimization system engineering tool for use with MATLAB, version 2.6," Dept. Elect. Comput. Eng., Purdue Univ., West Lafayette, IN, USA, Tech. Rep., Jan. 2014.

[33] J. A. Krizan and S. D. Sudhoff, "Theoretical performance boundaries for permanent magnet machines as a function of magnet type," in *Proc. IEEE Power Energy Soc. Gen. Meeting*, Jul. 2012, pp. 1–6, doi: 10.1109/PESGM.2012.6345224.

[34] J. Y. Alsawalhi and S. D. Sudhoff, "Design optimization of asymmetric salient permanent magnet synchronous machines," *IEEE Trans. Energy Convers.*, vol. 31, no. 4, pp. 1315–1324, Dec. 2016, doi: 10.1109/TEC.2016.2575138.

[35] J. A. Krizan and S. D. Sudhoff, "A design model for salient permanent-magnet machines with investigation of saliency and wide-speed-range performance," *IEEE Trans. Energy Convers.*, vol. 28, no. 1, pp. 95–105, Mar. 2013, doi: 10.1109/TEC.2012.2223699.

[36] A. E. Kasha and S. D. Sudhoff, "Multi-objective design optimization of a surface-mounted modular permanent-magnet pole machine," in *Proc. IEEE Power Energy Conf. Illinois (PECI)*, Urbana, IL, USA, Dec. 2016, pp. 1–7, doi: 10.1109/PECI.2016.7459229.

JESÚS R. PÉREZ-CARDONA received the B.S. degree in mechanical engineering from the University of Puerto Rico, Mayagüez Campus, in 2018, and the M.S. and Ph.D. degrees in environmental and ecological engineering from Purdue University, West Lafayette, IN, USA, in 2021, where he is currently pursuing the Ph.D. degree. His research interests include design and manufacturing for sustainability, manufacturing processes and systems, renewable energy systems, techno-economic assessment, life cycle assessment, and circular economy.

JOHN W. SUTHERLAND received the B.S. and M.S. degrees in industrial engineering and the Ph.D. degree in mechanical engineering from the University of Illinois at Urbana–Champaign. He is currently a Professor and the Fehsenfeld Family Head of Environmental and Ecological Engineering (EEE) with Purdue University. He has mentored more than 100 students to the completion of their graduate degrees and has published over 400 papers in various journals and conference proceedings. His research interests include the application of sustainability principles to design, manufacturing, and other industrial issues. He was a recipient of numerous national and international awards from SME, SAE, and ASME. He is a fellow of SME, ASME, CIRP, and AAAS.

SCOTT D. SUDHOFF (Fellow, IEEE) received the B.S. (Hons.), M.S., and Ph.D. degrees in electrical engineering from Purdue University in 1988, 1989, and 1991, respectively. From 1991 to 1993, he worked as a Consultant for P. C. Krause and Associates in aerospace power and actuation systems. From 1993 to 1997, he also worked as a Faculty Member with the University of Missouri–Rolla. In 1997, he joined as a Faculty Member with Purdue University, where he is currently the Michael and Katherine Birck Professor in electrical and computer engineering. His research interests include electric machinery, power electronics, marine and aerospace power systems, applied control, evolutionary computing, and genetic algorithms and their application to power electronic converter and electric machine design. He has published over 200 papers in these areas, including six prize papers. He served as the Editor-in-Chief for IEEE Transactions on Energy Conversion and IEEE Power and Energy Technology System Journal.

● ● ●